Deterministic Sampling with Separation of Variables in Spherical Coordinates

Daniel Frisch and **Uwe D. Hanebeck**
Intelligent Sensor-Actuator-Systems Laboratory (ISAS)
Institute for Anthropomatics and Robotics
Karlsruhe Institute of Technology (KIT), Germany
daniel.frisch@kit.edu, uwe.hanebeck@kit.edu

***Abstract*—Densities separable in spherical coordinates have two advantages: i) the normalization constant is easy to compute, as the cumulative distribution can be decomposed into individual scalar integrals, and ii) an orthogonal inverse transform is directly available via a simple, scalar initial value problem and can be used to compute deterministic samples. We propagate uniform low-discrepancy sequences through that orthogonal inverse transform and obtain very homogeneous and even visually appealing deterministic samples. To demonstrate this technique, we exemplarily propose some spherical-coordinate-separable densities in $\mathbb{S}^2$, $\mathbb{R}^2$, and $\mathbb{R}^3$, including a non-isotropic modification of the von Mises–Fisher distribution. The proposed densities may be used, e.g., to represent uncertain radar measurements and for directional estimation. Furthermore, the framework presented herein allows quite simple design of various more densities tailored to a given scenario.**

***Index Terms*—Deterministic sampling, directional estimation, orthogonal inverse transform sampling, von Mises–Fisher distribution, density design, numerical integration**

I. Introduction

A. Why Deterministic Sampling?

Sampling of various densities is an important tool in, e.g., state estimation and control, used to approximate intractable integrals, like expectations, occurring in prediction and filtering steps. Deterministic samples allow for reproducible results. Furthermore, since they are placed homogeneously, they also yield much faster convergence, i.e., comparable Monte Carlo results with fewer samples, compared to the slow $1/\sqrt{L}$ convergence of random samples.

B. Unscented Sampling

One deterministic sampling strategy is using a very small, fixed amount of samples matching the first two moments of the respective density. This is widely used in the Unscented Kalman Filter (UKF) in the Euclidean domain [1] and has also been proposed for spherical manifolds [2]. Yet often one wants to use more samples for increased accuracy. This may be achieved by adding more samples on the main axes, which has been proposed for the Gaussian density [3] as well as the Bingham density on the sphere [4], [5]. However, there still remain large gaps in between the main axes. They can be filled, at least for the isotropic von Mises–Fisher (vMF) density, with more "rays" of samples leading from the mode outwards, called an "orbit-planet" sample arrangement [6], [7]. Yet coverage is still unsatisfactory in some regions.

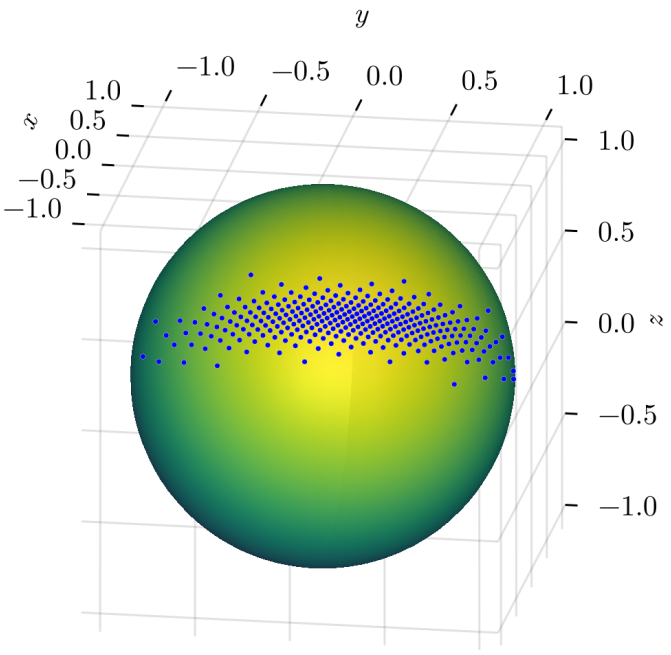

Fig. 1: 300 deterministic samples on the $\mathbb{S}^2$ sphere from the "von-Mises $\times$ von-Mises density", i.e., the product of two von-Mises densities over azimuth and elevation angles, which is an anisotropic modification (36) of the von Mises–Fisher density. Parameters: $\kappa_\theta = 120$, $\kappa_\varphi = 5$.

C. Optimization-Based Sampling

The "gold standard" to achieve homogenous coverage uses the Localized Cumulative Distribution (LCD) and numerical optimization to compute sample locations [8]. Again, this has been applied to the Gaussian density [9], [10] and sample reduction [11], the latter has also been adapted to the sphere [12], [13]. This method is, however, too slow for real-time application and requires suitable caching. A somewhat faster alternative is based on the projected cumulative distribution (PCD) [14], [15], with a gradient-free optimization procedure.

D. Transformation-Based Sampling

Finally, there is transformation-based Gaussian sampling [16], [17] which is very fast. In one scenario, 20 transformation-

based samples yielded the same accuracy as 200 random samples [17, Fig. 11b]. It is based on the idea that inverse transform sampling with generalized Fibonacci grids as uniform template samples yields homogeneous samples if the transform can be described via an orthogonal skeleton grid [18], [19, Sec. 6.7]. These points typically yield integration errors nearly as low as LCD-based samples while being much faster to compute. The same principle has already been applied to produce spherical vMF samples [20], and in this work, we are generalizing it to a much broader class of densities, where the vMF is just one example of.

E. Structure of the Paper

In Section III-A, will introduce uniform samples that are then transformed as described in Sections IV and V. Both the uniform template samples, as well as the transforms, must have special properties so that the desired homogeneity is achieved. Having laid out the fundamentals of the proposed framework, Section VI demonstrates various outcomes of homogeneous, deterministic samples of interesting densities.

II. Key Idea

For a given density f that is independent/separable in polar or spherical coordinates, find the separable inverse transform / quantile function Q. Take a uniform low-discrepancy point set $\mathcal{P}_L^{\mathrm{u}}$ of L samples, e.g., Fibonacci-based or Sobol. Then Q maps this point set into deterministic samples $\mathcal{P}_L^f$ of the desired density, $\mathcal{P}_L^f = Q(\mathcal{P}_L^{\mathrm{u}})$.

III. Uniform Low-Discrepancy Samples

We begin briefly introducing some uniform low-discrepancy point sets eligible to serve as template to be transformed to the desired densities later.

A. 2D: Kronecker–Fibonacci Lattice

For two-dimensional (2D) applications (here: $\mathbb{R}^2$ and $\mathbb{S}^2 \subset \mathbb{R}^3$), one may choose the Kronecker–Fibonacci lattice as low-discrepancy uniform template point set $\mathcal{P}_L^{\mathrm{u}}$ [21], [22]

$$\mathcal{P}_L^{\mathrm{u}} = \left\{ \begin{bmatrix} \frac{2i-1}{2L} \\ \frac{i}{\Phi} \mod 1 \end{bmatrix} \middle| \, i \in \{1, 2, \ldots, L\} \right\} , \tag{1}$$

with the inverse golden ratio [23, A094214]

$$\frac{1}{\Phi} = \frac{\sqrt{5}-1}{2} = 0.618033\ldots \ . \tag{2}$$

It is periodic along the coordinate with the modulo, i.e., the second coordinate in (1). This coordinate should therefore be chosen for the periodic spherical coordinate, i.e., p_2 in (10) and also p_2 in (19). If this is mixed up, an inhomogeneity can occur at the periodicity transition $2\pi \leftrightarrow 0$, see green samples in Fig. 2, centered horizontal line.

Unfortunately, there is currently no known equivalent of the Kronecker–Fibonacci lattice for dimensions higher than two [21, p. 222] with equivalent optimality *and* periodicity properties – only optimality *or* periodicity. Thus, for applications in, e.g., $\mathbb{R}^3$ or $\mathbb{S}^3$, we have to resort to alternatives.

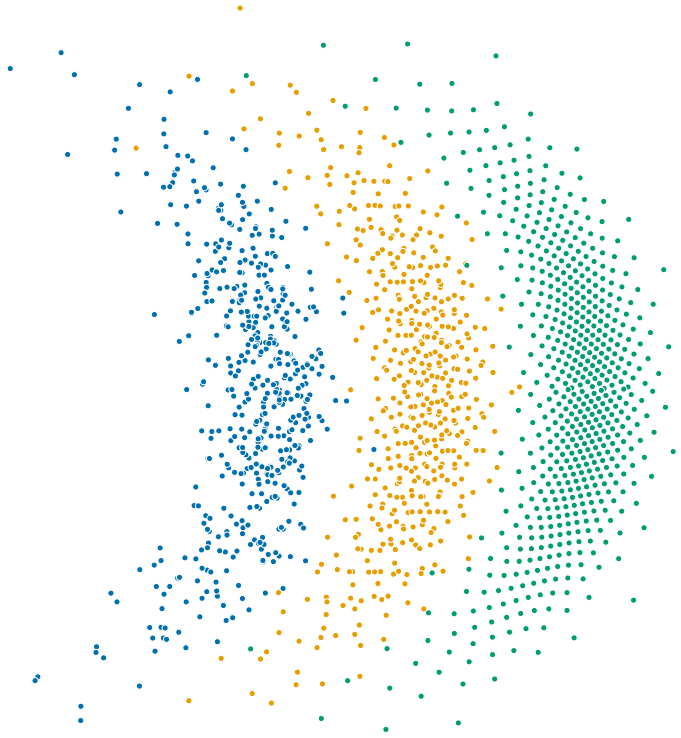

Fig. 2: Samples resulting from identical inverse transform but different uniform templates: random (blue), Sobol (yellow), and Kronecker–Fibonacci (green) however with aperiodic coordinate in (1) used for periodic coordinate φ in (10) – note the inhomogeneity along a horizontal line in the center in the green samples, compared to Section VI-A with the correct assignment. Density is von-Mises $\times$ truncated-Gauss with parameters $\kappa = 5,\ m_r = 5,\ \sigma_r = 0.5,\ L = 600$.

B. 3D: Frolov–Fibonacci Lattice

For three-dimensional (3D) applications (here: $\mathbb{R}^3$), one may choose the Frolov–Fibonacci lattice as proposed in [16], [17]. It can be constructed via

$$\mathcal{P}_L^{\mathrm{u}} = \left\{ \mathbf{V}^\top \cdot \delta \cdot \underline{z} \mid \underline{z} \in \mathbb{Z}^3 \right\} \cap [0,1]^3 \ , \tag{3}$$

where δ is chosen to obtain the desired L and $\mathbf{V}$ is the eigenvector matrix of the 3D quasi-Fibonacci matrix $\mathbf{M} = \left[\begin{smallmatrix} 1 & 1 & 1 \\ 1 & 1 & 0 \\ 1 & 0 & 0 \end{smallmatrix}\right]$. It is given in closed form by

$$\mathbf{V} = \sqrt{\frac{4}{7}} \begin{bmatrix} \cos\left(\frac{\pi}{14} \cdot 1\right) & \cos\left(\frac{\pi}{14} \cdot 3\right) & \cos\left(\frac{\pi}{14} \cdot 5\right) \\ \cos\left(\frac{\pi}{14} \cdot 3\right) & \cos\left(\frac{\pi}{14} \cdot 9\right) & \cos\left(\frac{\pi}{14} \cdot 15\right) \\ \cos\left(\frac{\pi}{14} \cdot 5\right) & \cos\left(\frac{\pi}{14} \cdot 15\right) & \cos\left(\frac{\pi}{14} \cdot 25\right) \end{bmatrix} . \tag{4}$$

For hints on how to implement (3) efficiently, refer to [17, Sec. IV.A].

A slight flaw of using Frolov lattices in the context of spherical coordinates is that Frolov lattices are not periodic. Thus, whenever significant probability mass is allocated all along a periodic coordinate (here: φ), the samples will not be deterministic/homogeneous at periodicity transitions $2\pi \leftrightarrow 0$.

C. 2D and 3D: Sobol

A well-known alternative to Fibonacci–based samples, with implementations readily available in all major languages, typically up to 1111 dimensions, is the Sobol sequence [24], [25]. This is a low-discrepancy point set that is periodic along all directions.

Although its discrepancy is much lower than for independent identically distributed (iid) random samples, it is not as low as that of Fibonacci-based samples. Therefore, the homogeneity of the resulting deterministic samples will be somewhat inferior, see yellow samples in Fig. 2.

IV. Orthogonal Inverse Transforms

Now we describe the general idea of inverse transforms of separable densities, starting with the rather simple polar coordinates in $\mathbb{R}^2$, using explicit notation, and progressing to $\mathbb{R}^3$ and $\mathbb{S}^2$. An even more basic introduction starting with the standard normal density in $\mathbb{R}$ has been given in [20].

A. $\mathbb{R}^2$ in Polar Coordinates

Given some density $f(\underline{x})$, $\underline{x} \in \mathbb{R}^2$ that is separable in polar coordinates, $f(r,\varphi) = f_r(r) \cdot f_\varphi(\varphi)$, and the polar "volume element" $\mathrm{d}V = r\,\mathrm{d}r\,\mathrm{d}\varphi$, we obtain the separable cumulative density function (CDF)

$$\begin{aligned} F(r,\varphi) &= \iint f(r,\varphi)\,\mathrm{d}V && (5)\\ &= \int_{r'=0}^{r}\int_{\varphi'=0}^{\varphi} f_r(r')\cdot f_\varphi(\varphi')\cdot r'\,\mathrm{d}r'\,\mathrm{d}\varphi' && (6)\\ &= \left(\int_0^r f_r(r')\cdot r'\,\mathrm{d}r'\right)\cdot\left(\int_0^\varphi f_\varphi(\varphi')\cdot\,\mathrm{d}\varphi'\right) && (7)\\ &= F_r(r)\cdot F_\varphi(\varphi)\ . && (8)\end{aligned}$$

Inversion gives us the quantile function that is identical to the desired separable inverse transform

$$Q_r(p_1) = F_r^{-1}(p_1) \qquad Q_\varphi(p_2) = F_\varphi^{-1}(p_2)\ , \tag{9}$$

or combined to a single function $Q\colon [0,1]^2 \mapsto \mathbb{R}^2$

$$Q\left(\begin{bmatrix}p_1\\p_2\end{bmatrix}\right) = \begin{bmatrix}F_r^{-1}(p_1)\\F_\varphi^{-1}(p_2)\end{bmatrix}\ . \tag{10}$$

To obtain samples $\mathcal{P}_L^f$ of f, insert uniform samples $\mathcal{P}_L^{\mathrm{u}}$ in (p_1,p_2). If those uniform samples are iid random, the resulting $\mathcal{P}_L^f$ will be iid as well. But if they are low-discrepancy, e.g., Kronecker–Fibonacci, the resulting $\mathcal{P}_L^f$ will be deterministic/homogeneous, see the difference in Fig. 2. The resulting samples are still in polar coordinates and may be transformed to Cartesian coordinates via $x = r\cdot\cos(\varphi)$, $y = r\cdot\sin(\varphi)$.

B. $\mathbb{R}^3$ in Spherical Coordinates

Given some density $f(\underline{x})$, $\underline{x} \in \mathbb{R}^3$ that is separable in spherical coordinates, $f(r,\theta,\varphi) = f_r(r)\cdot f_\theta(\theta)\cdot f_\varphi(\varphi)$, and the volume element $\mathrm{d}V = r^2\sin(\theta)\,\mathrm{d}r\,\mathrm{d}\theta\,\mathrm{d}\varphi$, we obtain the CDF

$$\begin{aligned} F(r,\theta,\varphi) &= \iiint f(r,\theta,\varphi)\,\mathrm{d}V\\ &= F_r(r)\cdot F_\theta(\theta)\cdot F_\varphi(\varphi)\ , \end{aligned} \tag{11}$$

where

$$F_r(r) = \int_{r'=0}^{r} f_r(r')\cdot(r')^2\,\mathrm{d}r'\ , \tag{12}$$

$$F_\theta(\theta) = \int_{\theta'=0}^{\theta} f_\theta(\theta')\cdot\sin(\theta')\,\mathrm{d}\theta'\ , \tag{13}$$

$$F_\varphi(\varphi) = \int_{\varphi'=0}^{\varphi} f_\varphi(\varphi')\,\mathrm{d}\varphi'\ . \tag{14}$$

The desired quantile functions are

$$\begin{aligned} Q_r(p_1) &= F_r^{-1}(p_1)\ ,\\ Q_\theta(p_2) &= F_\theta^{-1}(p_2)\ ,\\ Q_\varphi(p_3) &= F_\varphi^{-1}(p_3)\ . \end{aligned} \tag{15}$$

Again, inserting iid uniform samples produces iid samples of f, but inserting a low-discrepancy sequence, e.g., the Frolov–Fibonacci lattice, produces deterministic samples, all in spherical coordinates. Cartesian coordinates are obtained via

$$\begin{aligned} x &= r\cdot\sin(\theta)\cos(\varphi)\ ,\\ y &= r\cdot\sin(\theta)\sin(\varphi)\ ,\\ z &= r\cdot\cos(\theta)\ . \end{aligned} \tag{16}$$

C. $\mathbb{S}^2$ in Spherical Coordinates

Finally, we consider spherical densities $f(\underline{x})$, $\underline{x} \in \mathbb{S}^2 \subset \mathbb{R}^3$ separable in spherical coordinates $f(\theta,\varphi) = f_\theta(\theta)\cdot f_\varphi(\varphi)$. With the volume element $\mathrm{d}V = \sin(\theta)\,\mathrm{d}\theta\,\mathrm{d}\varphi$, we obtain the CDF

$$F(\theta,\varphi) = \iint f(\theta,\varphi)\,\mathrm{d}V = F_\theta(\theta)\cdot F_\varphi(\varphi)\ , \tag{17}$$

where

$$\begin{aligned} F_\theta(\theta) &= \int_{\theta'=0}^{\theta} f_\theta(\theta')\cdot\sin(\theta')\,\mathrm{d}\theta'\ ,\\ F_\varphi(\varphi) &= \int_{\varphi'=0}^{\varphi} f_\varphi(\varphi')\,\mathrm{d}\varphi'\ . \end{aligned} \tag{18}$$

The desired quantile functions are

$$Q_\theta(p_1) = F_\theta^{-1}(p_1)\ ,\quad Q_\varphi(p_2) = F_\varphi^{-1}(p_2)\ , \tag{19}$$

and Cartesian coordinates are (16) with $r = 1$.

V. Constructing Transformations Numerically

We have seen that evaluation of Q for inverse transform sampling comprises integration and inversion, so one may ask how to compute $\mathcal{P}_L^f = Q(\mathcal{P}_L^{\mathrm{u}})$ in practice. This section describes a range of such techniques.

A. Analytic Expression of Q

In some cases, integration and inversion can be performed in closed form, such that there is a closed form expression for Q, which can then be directly used as inverse transform. This is the case, e.g., with the vMF density on the $\mathbb{S}^2$ sphere [20].

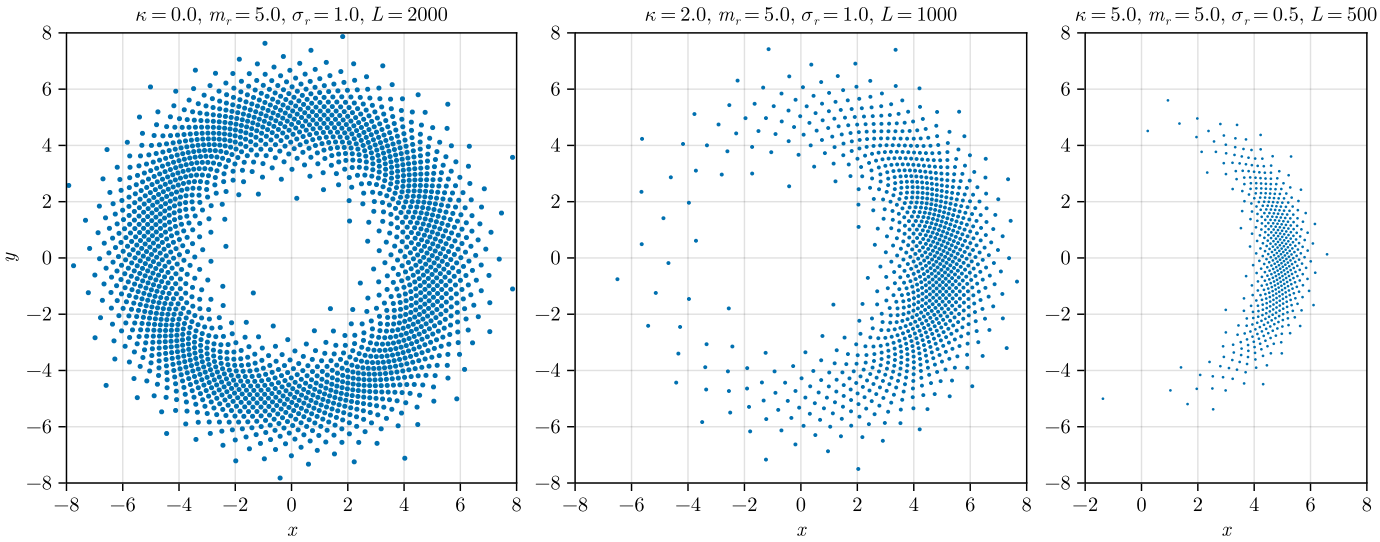

Fig. 3: Deterministic samples from the "von-Mises $\times$ truncated-Gaussian density" that is separable in polar coordinates, Section VI-A.

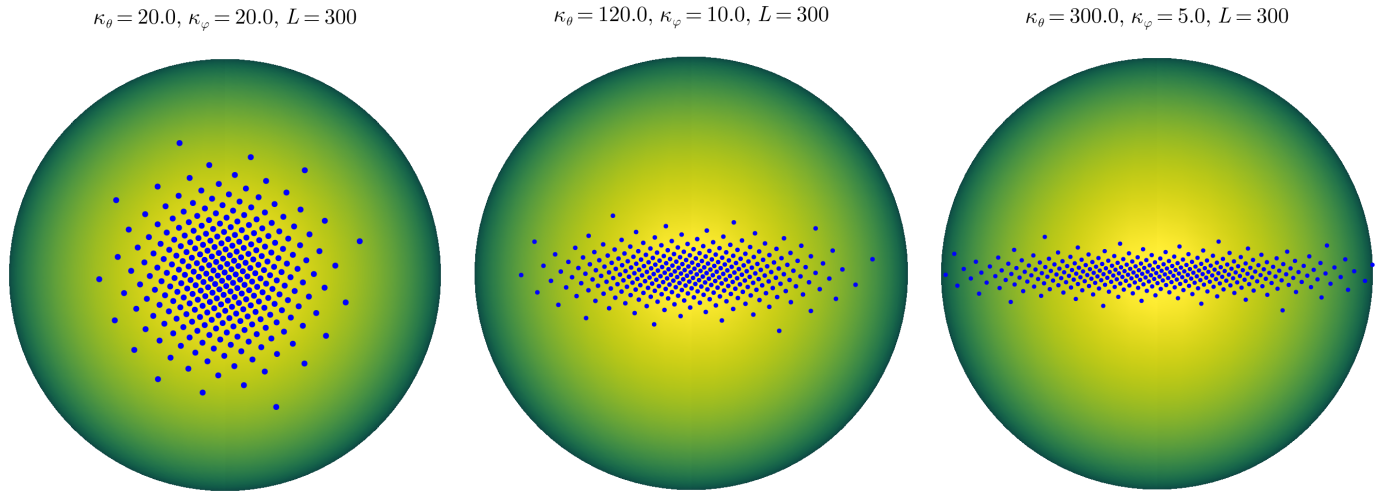

Fig. 4: Deterministic spherical / $\mathbb{S}^2$ samples from the "von-Mises $\times$ von-Mises density" (36) that is separable in spherical coordinates, Section VI-B.

B. Analytic Expression of F

In other cases, the cumulative F, i.e., the antiderivative of f, may be available in closed form but not its inverse function. Then we can solve

$$x_i = Q(p_i) \quad \Leftrightarrow \quad F(x_i) = p_i \tag{20}$$

for x_i numerically with the one-dimensional Newton-Raphson method or nested interval algorithms like bisection [26, Sec. II.C], [27, Sec. 9.1+9.4]. This is simplified by the fact that F is monotonic by definition.

C. Inverse Interpolation

Now we are considering cases where the antiderivative $F(x) = \int^x f(x')\,\mathrm{d}x'$ does not exist in closed form, i.e., we only have an expression or a function handle of f. We can then formulate an ordinary differential equation (ODE)

$$F'(x) = f(x) \ , \qquad F(0) = 0 \ , \tag{21}$$

and compute F with numerical ODE / initial value problem solvers. Translated to the typical language in ODE solver documentations, this reads

$$u'(t) = f(t) \ , \qquad u(0) = 0 \ , \tag{22}$$

where $u \equiv F$ and $t \equiv x$. The solver provides a list of (t, u)-tuples representing F. If we interchange the coordinates and interpolate the (u, t)-tuples, we obtain an approximation of the desired Q [19, Sec. 7.4.3]. This constitutes a tabulation of Q that we can employ repeatedly. With this method, f also does not need to be normalized, as we obtain the normalization constant as the last value of u.

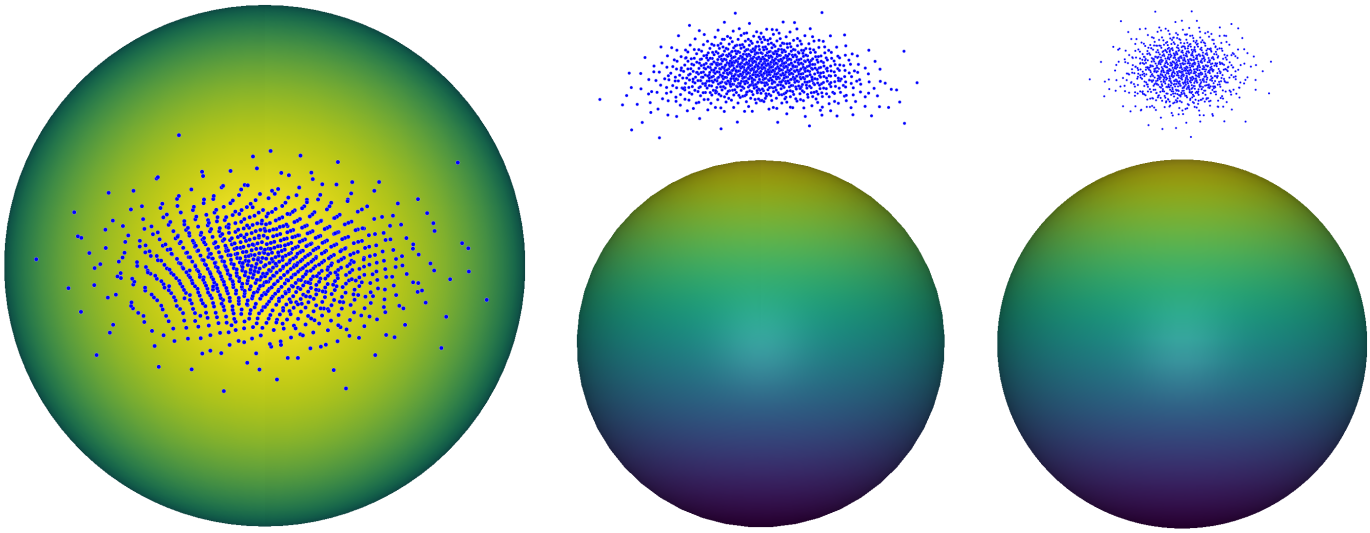

Fig. 5: Deterministic samples in $\mathbb{R}^3$ from the "von-Mises $\times$ von-Mises $\times$ truncated-Gaussian density" that is separable in spherical coordinates, Section VI-C, seen from three different perspectives (left to right: view on yz-plane, xy-plane, xz-plane). Parameters are $\kappa_\theta = 100,\ \kappa_\varphi = 30,\ m_r = 1.5,\ \sigma_r = 0.1,\ L = 1000$. Uniform template is Frolov–Fibonacci.

D. Inverse ODE

Finally, we can write Q directly as an ODE in terms of f, entirely skipping F as an intermediate result

$$u'(t) = \frac{1}{f(u)} \ , \qquad u(0) = 0 \ , \qquad t \in [0,1] \ , \tag{23}$$

where $u \equiv Q$ [19, Sec. 7.4.3]. This follows from the inverse function theorem and can be shown with a simple proof:

$$F(Q(p)) = p \qquad | \ \frac{\partial}{\partial p} \tag{24}$$

$$F'(Q(p)) \cdot Q'(p) = 1 \qquad | \ F'(x) = f(x) \tag{25}$$

$$f(Q(p)) \cdot Q'(p) = 1 \qquad | \ \text{solve for } Q' \tag{26}$$

$$Q'(p) = \frac{1}{f(Q(p))} \ . \tag{27}$$

However, this method can only be applied in regions where the integrand is strictly positive.

VI. Examples

Putting it all together, we state some interesting examples, one for each of the domains described in Section IV, respectively.

A. $\mathbb{R}^2$: Von-Mises $\times$ Truncated-Gaussian Density

As a model density separable in polar coordinates (described in Section IV-A), we choose a von Mises density f_φ along the angular coordinate $\varphi \in [0, 2\pi)$

$$\begin{aligned} f_\varphi(\varphi) &= c_\varphi^{-1} \cdot \exp\{\kappa \cdot \cos(\varphi)\} \ , \\ c_\varphi &= 2\pi I_0(\kappa) \ , \end{aligned} \tag{28}$$

where I_0 is the zeroth-order modified Bessel function of the first kind, and a truncated normal distribution $f_r(r)$ along the radial coordinate $r \geq 0$

$$\begin{aligned} f_r(r) &= c_r^{-1} \cdot \exp\left\{ -\frac{1}{2}\left(\frac{r - m_r}{\sigma_r}\right)^2 \right\} \ , \\ c_r &= \sqrt{\frac{\pi}{2}}\, m_r\, \sigma_r \cdot \left(2 + \frac{1}{2\sqrt{\pi}} \cdot \Gamma\left(-\frac{1}{2}, \frac{m_r^2}{2\,\sigma_r^2}\right)\right) \ , \end{aligned} \tag{29}$$

where Γ is the upper incomplete gamma function. The parameter $\kappa \geq 0$ quantifies angular uncertainty, $\sigma_r > 0$ radial uncertainty, and $m_r \geq 0$ the radial mode. For example, imagine f_r encoding the uncertain distance measurement and f_φ the angular measurement of a radar system.

The angular quantile function Q_φ is not available in closed form but can be computed following Section V-D by solving the scalar initial value problem

$$u'(t) = \frac{1}{f_\varphi(u)} \ , \qquad u(0) = 0 \ , \qquad t \in [0,1] \ , \tag{30}$$

with f_φ from (28) and $u \equiv Q_\varphi$. The radial cumulative

$$F_r(r) = \int_{r'=0}^{r} f_r(r') \cdot r' \, \mathrm{d}r' \ , \tag{31}$$

note the additional factor r' from (7), is available in closed form via

$$\begin{aligned} &F_r(r) \cdot c_r = \\ &\sigma_r^2 \cdot \left[\exp\left\{ -\frac{1}{2}\left(\frac{m_r}{\sigma_r}\right)^2 \right\} - \exp\left\{ -\frac{1}{2}\left(\frac{m_r - r}{\sigma_r}\right)^2 \right\} \right] \\ &+ \sqrt{\frac{\pi}{2}}\, m_r\, \sigma_r \cdot \left[\operatorname{erf}\left(\frac{m_r}{\sqrt{2}\,\sigma_r}\right) - \operatorname{erf}\left(\frac{m_r - r}{\sqrt{2}\,\sigma_r}\right) \right] \ , \end{aligned} \tag{32}$$

but not its inverse. Thus, it may be solved via bisection as described in Section V-B.

Now we can insert into Q the uniform low-discrepancy Kronecker–Fibonacci points $\mathcal{P}_L^{\mathrm{u}}$ from Section III-A. The angular coordinates become

$$\varphi_i = Q_\varphi\left(\frac{i}{\Phi} \mod 1\right) = u\left(\frac{i}{\Phi} \mod 1\right) \ , \qquad (33)$$

where u is the solution of (30), for $i \in \{1, 2, \ldots, L\}$. The radial coordinates r_i are obtained by solving

$$\frac{2i-1}{L} = F_r(r_i) \ , \qquad (34)$$

via bisection, with $F_r(r)$ from (32). This gives deterministic samples $\mathcal{P}_L^f$ of f in polar coordinates; the same samples in Cartesian coordinates are finally $x_i = r_i \cdot \cos(\varphi_i)$, $y_i = r_i \cdot \sin(\varphi_i)$. Computation of (33) with `DifferentialEquations.jl` [28] and (34) with `Roots.jl` took about 0.25 ms and 9 ms on a desktop computer for 2000 samples without parallelization. See Fig. 3 for visual examples.

B. $\mathbb{S}^2$: *Von-Mises* $\times$ *Von-Mises Density*

We already published this method with a density that would fit here, namely the vMF density [20]

$$f(\theta) = c^{-1} \cdot \exp\{\kappa \cdot \cos(\theta)\} \ , \quad c = 4\pi \, \frac{\sinh(\kappa)}{\kappa} \ . \qquad (35)$$

In this notation with a fixed mean direction at $\theta = 0$, and because it is isotropic, the density depends only on θ and not on φ, therefore both coordinates are independent – but as a rather trivial case.

Now we propose a different spherical density on $\mathbb{S}^2 \subset \mathbb{R}^3$ that is separable in spherical coordinates, non-isotropic, and depends on both θ and φ,

$$\begin{aligned} f(\theta, \varphi) &= c_\theta^{-1} c_\varphi^{-1} \cdot \exp\{\kappa_\theta \cdot \sin(\theta) + \kappa_\varphi \cdot \cos(\varphi)\} \ , \\ c_\theta &= \pi \cdot [I_1(\kappa_\theta) + \mathbf{L}_{-1}(\kappa_\theta)] \ , \\ c_\varphi &= 2\pi \, I_0(\kappa_\varphi) \ , \end{aligned} \qquad (36)$$

where I_n is the n^{th}-order modified Bessel function of the first kind, and $\mathbf{L}$ the modified Struve function.

For intuition, note that the standard vMF "kernel" $\exp\{\kappa \cdot \cos(\theta - \theta_0)\}$ has, for small uncertainties, the same shape as the Gaussian kernel $\exp\{-\frac{1}{2}(x - x_0)^2\}$ [12, Fig. 2]. And just like a 2D Gaussian is obtained by multiplying two univariate Gaussians, $\exp\{-\frac{1}{2}((x - y_0)^2 + (y - y_0)^2)\}$, we propose multiplying one vMF kernel along θ (around $\theta_0 = \pi/2$) with a second one along φ (here around $\varphi_0 = 0$), yielding $\exp\{\cos(\theta - \pi/2) + \cos(\varphi)\}$, leading to (36).

Cumulatives F are not available in closed form, neither is the inverse ODE method from Section V-D suitable due to division by zero. Instead, we use the inverse interpolation method from Section V-C. That is, we solve the initial value problem

$$\begin{aligned} u' &= c_\theta^{-1} \cdot \exp\{\kappa_\theta \cdot \sin(t)\} \cdot \sin(t) \ , \\ u(0) &= 0 \ , \quad t \in [0, \pi] \ , \end{aligned} \qquad (37)$$

yielding a list of (t, u)-tuples representing $F : t \mapsto u$, and set up the inverse interpolation function employing the (u, t)-tuples representing $Q : u \mapsto t$. We insert the non-periodic coordinate of the Kronecker–Fibonacci lattice $\left(\frac{2i-1}{2L}\right)$ as evaluation points (corresponding to u), then the interpolated t are the θ coordinates of $\mathcal{P}_L^f$. Similarly for the φ coordinates, we solve the initial value problem

$$\begin{aligned} u' &= c_\varphi^{-1} \cdot \exp\{\kappa_\varphi \cdot \cos(\varphi)\} \ , \\ u(0) &= 0 \ , \quad t \in [0, 2\pi] \ , \end{aligned} \qquad (38)$$

set up the inverse interpolation function $u \mapsto t$, insert the periodic Kronecker–Fibonacci coordinate $(\frac{i}{\Phi} \mod 1)$, and out comes the φ coordinate. The desired Cartesian coordinates of $\mathcal{P}_L^f$ are obtained through (16) with $r = 1$. Solving one ODE took about 0.08 ms on a desktop computer. The current restriction on the density's main direction and the orientation of its main axes can be remedied by transforming the Cartesian coordinates with a suitable rotation matrix. See Figs. 1 and 4 for visual examples (without the rotation matrix).

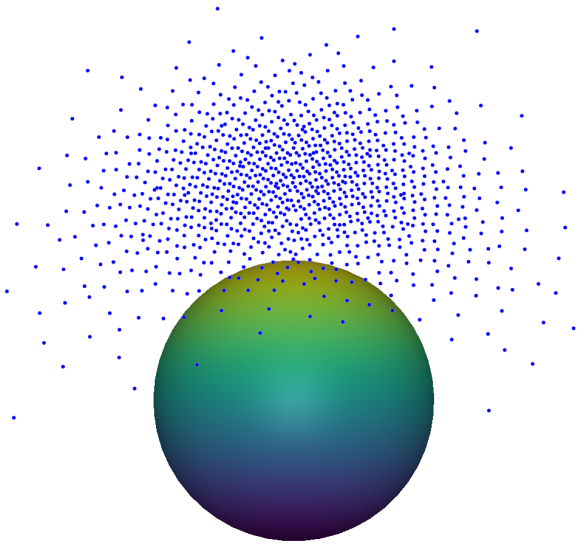

Fig. 6: Same as Fig. 5, but different parameters: $\kappa_\theta = 200$, $\kappa_\varphi = 5$, $m_r = 1.5$, $\sigma_r = 0.4$, $L = 1000$.

C. $\mathbb{R}^3$: *Von-Mises* $\times$ *Von-Mises* $\times$ *Truncated-Gaussian Density*

We can make a spherical density "leave the sphere" by augmenting it with a radial component. Here, we take the $\mathbb{S}^2 \subset \mathbb{R}^3$ density from (36) and augment it with the truncated normal distribution (29) as radial component f_r, yielding an $\mathbb{R}^3$ density. The the now different normalization constant of f_r (due to the r^2 factor) is

$$\begin{aligned} c_r = m_r \, \sigma_r^2 \exp\left\{-\frac{1}{2}\left(\frac{m_r}{\sigma_r}\right)^2\right\} \\ + \sqrt{\frac{\pi}{2}} \, \sigma_r \cdot (m_r^2 + \sigma_r^2) \cdot \left(1 + \operatorname{erf}\left(\frac{m_r}{\sqrt{2}\,\sigma_r}\right)\right) \ . \end{aligned} \qquad (39)$$

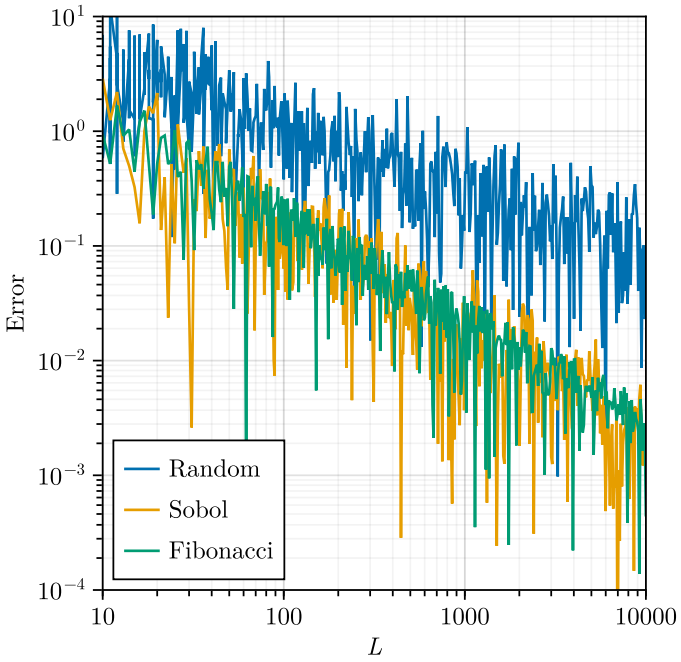

Fig. 7: Evaluation for Monte Carlo integration with the proposed samples (Fibonacci, Sobol) and conventional iid samples (Random). Shown is the absolute integration error.

Again the cumulative $F_r(r) = \int_{r'=0}^{r} f_r(r') \cdot (r')^2 \,\mathrm{d}r'$ is available in closed form via

$$F_r(r) \cdot c_r = \sigma_r^2 \, e^{-\frac{m_r^2+r^2}{2\sigma_r^2}} \left(m_r \, e^{\frac{r^2}{2\sigma_r^2}} - (m_r + r) \, e^{\frac{m_r r}{\sigma_r^2}} \right) + \\ \sqrt{\frac{\pi}{2}} \, \sigma_r \cdot (m_r^2 + \sigma_r^2) \left(\operatorname{erf}\left(\frac{m_r}{\sqrt{2}\,\sigma_r} \right) - \operatorname{erf}\left(\frac{m_r - r}{\sqrt{2}\,\sigma_r} \right) \right) . \tag{40}$$

The θ and φ coordinates are obtained just as described in Section VI-B – only that we insert, instead of the 2D Kronecker–Fibonacci lattice, now the 3D Kronecker–Frolov lattice from Section III-B (or alternatively the Sobol sequence). The r coordinates r_i are computed by solving $F_r(r_i) = p_i$ via bisection, with F_r from (40) and p_i one coordinate from the Kronecker–Frolov lattice or Sobol sequence. Mapping to Cartesian coordinates is done with (16). Solving the ODEs took about $0.07\,\mathrm{ms}$ each, and the bisection $10\,\mathrm{ms}$, for 2000 samples. See Figs. 5 and 6 for visual examples.

VII. Evaluation

For evaluation, we define the function $g(\underline{x}) = (x_1 - m_1)^3 + (x_2 - m_2)^3$, $\underline{m} = [1, 2]^\top$, and approximate the expectation integral, $\iint_{\mathbb{R}^2} g(\underline{x}) \cdot f(\underline{x}) \,\mathrm{d}\underline{x} = -16.844\ldots$, where f is the von-Mises $\times$ truncated-Gaussian density from Section VI-A with parameters $\kappa = 0$, $m_r = 1$, and $\sigma_r = 0.5$, with Monte Carlo sample approximations, $\frac{1}{L} \sum_{x \in \mathcal{P}_L^f} g(\underline{x})$, with various L and variants of template samples. See Fig. 7 for the results. The deterministic samples show a much faster convergence rate. For example, the integration error 0.1 can be achieved either with about 200 deterministic or 6000 random samples.

VIII. Conclusion

We demonstrated that the class of spherical-coordinate-separable densities is very expressive, and that it is quite easy to formulate one such density that is tailored to the particular application at hand – be it representing uncertain radar or sonar measurements, wind directions, or robotic actuators. We demonstrated this with three particular exemplaric densities, among them a very interesting non-isotropic modification of the von Mises–Fisher distribution (36), see Fig. 4. Our main focus lies on drawing homogeneous deterministic samples from those densities – that also turn out to be visually appealing in the $\mathbb{R}^2$ and $\mathbb{S}^2$ case if the Kronecker–Fibonacci lattice is used as uniform template. The deterministic sampling is achieved via an orthogonal inverse transform, facilitated by the separability, using low-discrepancy sequences as uniform template particles. In the future, we are seeking to generalize (36) to higher dimensions: in $\mathbb{S}^3$ it could well represent uncertain quaternions and serve as an alternative to the Bingham density in directional estimation.

References

[1] Simon J. Julier and Jeffrey K. Uhlmann. "New Extension of the Kalman Filter to Nonlinear Systems". In: *Signal Processing, Sensor Fusion, and Target Recognition VI*. Vol. 3068. International Society for Optics and Photonics. July 1997, pp. 182–193.

[2] Gerhard Kurz, Igor Gilitschenski, and Uwe D. Hanebeck. "Unscented von Mises–Fisher Filtering". In: *IEEE Signal Processing Letters* 23.4 (Apr. 2016), pp. 463–467. DOI: 10.1109/LSP.2016.2529854.

[3] Marco F. Huber and Uwe D. Hanebeck. "Gaussian Filter based on Deterministic Sampling for High Quality Nonlinear Estimation". In: *Proceedings of the 17th IFAC World Congress (IFAC 2008)*. Vol. 17. 2. Seoul, Republic of Korea, July 2008. DOI: 10.3182/20080706-5-KR-1001.02291.

[4] Kailai Li, Daniel Frisch, Benjamin Noack, and Uwe D. Hanebeck. "Geometry-Driven Deterministic Sampling for Nonlinear Bingham Filtering". In: *Proceedings of the 2019 European Control Conference (ECC 2019)*. Naples, Italy, June 2019. DOI: 10.23919/ECC.2019.8796102.

[5] Kailai Li, Florian Pfaff, and Uwe D. Hanebeck. "Hyperspherical Deterministic Sampling Based on Riemannian Geometry for Improved Nonlinear Bingham Filtering". In: *Proceedings of the 22nd International Conference on Information Fusion (Fusion 2019)*. Ottawa, Canada, July 2019. DOI: 10.23919/FUSION43075.2019.9011390.

[6] Kailai Li, Florian Pfaff, and Uwe D. Hanebeck. "Nonlinear von Mises–Fisher Filtering Based on Isotropic Deterministic Sampling". In: *Proceedings of the 2020 IEEE International Conference on Multisensor Fusion and Integration for Intelligent Systems (MFI 2020)*. Virtual, Sept. 2020. DOI: 10.1109/MFI49285.2020.9235260.

[7] Kailai Li, Florian Pfaff, and Uwe D. Hanebeck. "Progressive von Mises–Fisher Filtering Using Isotropic Sample Sets for Nonlinear Hyperspherical Estimation". In: *Sensors* (Apr. 2021). DOI: 10.3390/s21092991.

[8] Uwe D. Hanebeck and Vesa Klumpp. "Localized Cumulative Distributions and a Multivariate Generalization of the Cramér-von Mises Distance". In: *Proceedings of the 2008 IEEE International Conference on Multisensor Fusion and Integration for Intelligent Systems (MFI 2008)*. Seoul, Republic of Korea, Aug. 2008, pp. 33–39. DOI: 10.1109/MFI.2008.4648104.

[9] Uwe D. Hanebeck, Marco F. Huber, and Vesa Klumpp. "Dirac Mixture Approximation of Multivariate Gaussian Densities". In: *Proceedings of the 2009 IEEE Conference on Decision and Control (CDC 2009)*. Shanghai, China, Dec. 2009. DOI: 10.1109/CDC.2009.5400649.

[10] Jannik Steinbring, Martin Pander, and Uwe D. Hanebeck. "The Smart Sampling Kalman Filter with Symmetric Samples". In: *Journal of Advances in Information Fusion* 11.1 (June 2016), pp. 71–90.

[11] Uwe D. Hanebeck. "Optimal Reduction of Multivariate Dirac Mixture Densities". In: *at – Automatisierungstechnik* 63.4 (Apr. 2015), pp. 265–278. DOI: 10.1515/auto-2015-0005.

[12] Daniel Frisch, Kailai Li, and Uwe D. Hanebeck. "Optimal Reduction of Dirac Mixture Densities on the 2-Sphere". In: *Proceedings of the 1st Virtual IFAC World Congress (IFAC-V 2020)*. July 2020. DOI: 10.1016/j.ifacol.2020.12.1856.

[13] Kailai Li, Florian Pfaff, and Uwe D. Hanebeck. "Hyperspherical Dirac Mixture Reapproximation". In: *arXiv preprint arXiv:2110.10411* (Oct. 2021).

[14] Uwe D. Hanebeck. "Deterministic Sampling of Multivariate Densities based on Projected Cumulative Distributions". In: *Proceedings of the 54th Annual Conference on Information Sciences and Systems (CISS 2020)*. Princeton, New Jersey, USA, Mar. 2020. DOI: 10.1109/CISS48834.2020.1570617413.

[15] Dominik Prossel and Uwe D. Hanebeck. "Dirac Mixture Reduction Using Wasserstein Distances on Projected Cumulative Distributions". In: *Proceedings of the 25th International Conference on Information Fusion (Fusion 2022)*. Linköping, Sweden, July 2022. DOI: 10.23919/FUSION49751.2022.9841285.

[16] Daniel Frisch and Uwe D. Hanebeck. "Deterministic Gaussian Sampling With Generalized Fibonacci Grids". In: *Proceedings of the 24th International Conference on Information Fusion (Fusion 2021)*. Sun City, South Africa, Nov. 2021. DOI: 10.23919/FUSION49465.2021.9626975.

[17] Daniel Frisch and Uwe D. Hanebeck. "The Generalized Fibonacci Grid as Low-Discrepancy Point Set for Optimal Deterministic Gaussian Sampling". In: *Journal of Advances in Information Fusion* 18.1 (June 2023), pp. 16–34. ISSN: 1557-6418.

[18] Robert James Purser. *Generalized Fibonacci Grids; A New Class of Structured, Smoothly Adaptive Multi-Dimensional Computational Lattices*. May 2008.

[19] Daniel Frisch. "Transformable Deterministic Sampling". PhD thesis. Karlsruher Institut für Technologie (KIT), 2025. 301 pp. DOI: 10.5445/IR/1000179985.

[20] Daniel Frisch and Uwe D. Hanebeck. "Deterministic Von Mises-Fisher Sampling on the Sphere Using Fibonacci Lattices". In: *Proceedings of the combined IEEE 2023 Symposium Sensor Data Fusion and International Conference on Multisensor Fusion and Integration (SDF-MFI 2023)*. Bonn, Germany, Nov. 2023. DOI: 10.1109/SDF-MFI59545.2023.10361396.

[21] Harald Niederreiter and Arne Winterhof. *Applied Number Theory*. en. Cham: Springer International Publishing, Sept. 2015. ISBN: 978-3-319-22321-6. DOI: 10.1007/978-3-319-22321-6.

[22] Josef Dick, Frances Y. Kuo, and Ian H. Sloan. "High-Dimensional Integration: The Quasi-Monte Carlo Way". In: *Acta Numerica* 22 (2013), pp. 133–288. DOI: 10.1017/S0962492913000044.

[23] OEIS Foundation, Inc. *The On-Line Encyclopedia of Integer Sequences*. Published electronically at http://oeis.org. 2023.

[24] Stephen Joe and Frances Y. Kuo. "Remark on Algorithm 659: Implementing Sobol's Quasirandom Sequence Generator". In: *ACM Trans. Math. Softw.* 29.1 (Mar. 2003), pp. 49–57. ISSN: 0098-3500. DOI: 10.1145/641876.641879.

[25] I.M. Sobol. "Uniformly Distributed Sequences with an Additional Uniform Property". In: *USSR Computational Mathematics and Mathematical Physics* 16.5 (1976), pp. 236–242. ISSN: 0041-5553. DOI: https://doi.org/10.1016/0041-5553(76)90154-3.

[26] Gerhard Kurz and Uwe D. Hanebeck. "Stochastic Sampling of the Hyperspherical von Mises–Fisher Distribution Without Rejection Methods". In: *Proceedings of the IEEE ISIF Workshop on Sensor Data Fusion: Trends, Solutions, Applications (SDF 2015)*. Bonn, Germany, Oct. 2015. DOI: 10.1109/SDF.2015.7347705.

[27] William H. Press, Saul A. Teukolsky, William T. Vetterling, and Brian P. Flannery. *Numerical Recipes 3rd Edition: The Art of Scientific Computing*. Cambridge university press, 2007.

[28] Christopher Rackauckas and Qing Nie. "DifferentialEquations.jl–a Performant and Feature-Rich Ecosystem for Solving Differential Equations in Julia". In: *Journal of Open Research Software* 5.1 (2017).